BAROCLINIC WAVE TRANSITIONS IN THE MARTIAN ATMOSPHERE.

M. Collins, S.R. Lewis, P.L. Read

Atmospheric, Oceanic and Planetary Physics,

Clarendon Laboratory,

Parks Road,

Oxford,

UK,

OX1 3PU.

Tel: 44 1865 272933

Fax: 44 1865 272923

Email: collins@atm.ox.ac.uk, lewis@atm.ox.ac.uk, read@atm.ox.ac.uk

and F. Hourdin

Laboratoire de Météorologie Dynamique du CNRS,

Ecole Normale Supérieure,

24 rue Lhomond,

75 231,

Paris Cedex 05,

France.

Tel: 33 1 44 32 22 47

Fax: 33 1 43 36 83 92

Email: hourdin@lmd.ens.fr

31 Pages.

16 figures.

0 Tables.

Key words: ATMOSPHERES, DYNAMICS, MARS, METEOROLOGY.

Proposed running head: MARTIAN BAROCLINIC WAVES.

Corresponding Author:

Matthew Collins,

Atmospheric, Oceanic and Planetary Physics,

Clarendon Laboratory,

Parks Road,

Oxford,

UK,

OX1 3PU.

Tel: 44 1865 272086

Fax: 44 1865 272923

Email: collins@atm.ox.ac.uk

Abstract

Surface pressure data from the Viking Lander mission and from GCM simulations of the Martian atmosphere have been analysed using singular systems analysis. Very regular oscillations are found with frequencies that are are distributed bimodally with peaks corresponding to periods of approximately 2-4 days and 5-7 days respectively. Reconstructions of the amplitudes of the two oscillations are often negatively correlated, i.e. when the amplitude of one oscillation is large that of the other is small. The GCM simulations show that the negative correlation in the amplitudes of the two oscillations can be explained as a flipping between two different wavenumber modes. In the absence of diurnal forcing in the model, transition from an unrealistically regular high frequency mode to a similarly unrealistic regular low frequency mode occurs at most once during the northern winter season. The diurnal cycle in the model, however, acts in a non-linear sense to stimulate the transitions between the two wavenumbers and thus increases the frequency of mode flipping events. The corresponding simulations bear a closer resemblance to the observations.

1 Introduction

The existence of baroclinic transient waves (or weather systems) in the Martian atmosphere had long been suspected since the work of Hess (1950), but was put on a firm footing by Barnes (1980,1981). Barnes showed that measurements of pressure, temperature, wind speed and wind direction from the meteorological package aboard Viking Lander 2 (hereafter VL2, Chamberlain *et al.* (1976)), situated at 48° N 226° W on the planet, showed oscillations with phase relationships consistent with those found in terrestrial baroclinic waves and those predicted by earlier analytic (Leovy (1969), Gadian (1978)) and numerical studies (Leovy and Mintz (1969)). Figure 1 shows the surface pressure from VL2 with the data binned 25 times per Martian day from the entire mission (henceforth, day shall refer to a Martian day which is 24h 37m). The biggest data gap occurred from around day 560 to day 630 of the mission, whilst smaller data gaps occured throughout, but more frequently during the second year. The large amplitude seasonal cycle of pressure is due mainly to the exchange of CO_2 between the surface and the atmosphere, but also partly due to changes in the large scale circulation patterns (Hourdin *et al.* (1993)). Shorter time scale oscillations are due to baroclinic waves (Barnes 1980,1981) and thermal tides (Zurek (1988)). The data was obtained from the Atmospheres node of the Planetary Data System database (e-mail lee@syrtis.colorado.edu).

Using this and other data taken from the second Martian year of measurement, Barnes (1981) also showed that the oscillations of meteorological variables, in the frequency range appropriate for Martian baroclinic waves, were often very regular and repeatable, that is, with significantly peaked frequency spectra. Figure 2 shows the frequency spectrum of a detrended version of the data shown in fig. 1 computed using Fourier analysis for frequencies in the range 0 to 1.1 $(day)^{-1}$. The dotted line represents the 95% confidence limits based on a red noise spectrum with the same variance and lag one autocorrelation coefficient as the observed data. The spectral peaks that occur above this line are at periods of 8.0, 7.1, 3.5, 3.4, 3.0, 2.3, 2.2 and 1.0 Martian days. The large peak at 1.0 days is due to the diurnal cycle which is at its strongest during the summer seasons. Sharman and Ryan (1980) performed a similar analysis on the daily averaged pressure from the first year of measurement whilst Barnes (1980,1981) showed frequency spectra calculated from shorter segments of the time series. The peaking of the spectrum is in contrast to spectra from similar terrestrial measurements which generally have flat, rather red shapes with no significant peaks (e.g. Hartmann (1974)). This has lead to the suggestion that Martian weather systems are much more regular and coherent than corresponding weather systems on the Earth where weather forecasts often lose predictability after only a few days.

Theoretical studies of Martian baroclinic waves have tended to focus on linear instability studies (Gadian (1978), Barnes (1984)), highly truncated non-linear models (Barnes (1986)) and diagnostic studies of full GCMs (Pollack *et al.* (1981), Barnes *et al.* (1993)). More recently, Collins and James (1995) have used a fully non-linear GCM with simplified parametrisations of physical processes, namely Newtonian cooling and Rayleigh friction, to examine the regular nature of baroclinic waves in the context of Mars. They found that for certain parameter settings, corresponding to those representative of the Martian atmosphere, large amplitude regular waves were excited in the model. These regular waves are in stark contrast to irregular waves seen in similar terrestrial studies (James and James (1992)) and seen on a day to day basis in the Earth's troposphere. Collins and James concluded that the short radiative time scale in the Martian atmosphere, and hence large heating and cooling rates, resulted in a complicated non-linear balance between advection and diabatic heating, thus maintaining the large amplitude waves. It is the radiative relaxation time scale therefore which seems to be at least one of the crucial parameters that leads to Martian baroclinic waves being regular and terrestrial baroclinic waves being irregular and possibly chaotic.

In this paper we have used a novel analysis technique adopted by Fraedrich (1986) and Broomhead and King (1986), to analyse simulated VL2 data taken from several Martian GCM experiments and to re-examine the observed VL2 surface pressure data . Section 2 describes the analysis technique, namely singular systems analysis (SSA). Section 3 of the paper briefly describes the GCM used in the study. Section 4 shows the results of applying the technique to the observed VL2 pressure data. Sections 5 and 6 describe what was found when the analysis was applied to simulated VL2 data from various GCM experiments and finally, the results are discussed and a proposed interpretation is put forward in section 7.

2 Singular Systems Analysis

Singular systems analysis (SSA) was pioneered by Fraedrich (1986) and Broomhead and King (1986) in the context of the analysis of time series. Given a uniformly sampled time series of a variable with zero mean,

$$\{x\} = x_1, x_2, ..., x_N, \tag{1}$$

one can form a series of vectors,

$$\mathbf{x}_i \;=\; (x_i, x_{i+k}, x_{i+2k}, ..., x_{i+(M-1)k}) \quad i \;=\; 1, N - kM. \tag{2}$$

These vectors are called the time delay vectors and are often described as being formed by sliding a window of length kM along the time series. We then form the $M \times M$ covariance matrix $\mathbf{C}$ from these vectors whose $(i,j)^{th}$ element c_{ij} is the quantity

$$c_{ij} \;=\; \frac{1}{NM} \; < \mathbf{x}_i \cdot \mathbf{x}_j >, \tag{3}$$

where the angled brackets denote a time average. Note that the trace of the matrix is equal to the total variance of the time series. SSA then involves finding the eigenvalues and eigenvectors of this (real symmetric) matrix and ordering the eigenvalues with decreasing magnitude, thus partitioning the series variance. We say that the eigenvector corresponding to a particular eigenvalue *explains* a certain percentage of the variance associated with that eigenvalue. Because we have ordered the eigenvalues in monotonically decreasing order the first eigenvector explains the most variance, the second eigenvector explains the second largest amount of variance and so on. We thus form an orthonormal basis for the time series that is optimal in the sense that if we reconstruct the time series from a combination of the first n eigenvectors, the reconstructed series will contain the largest fraction of the variance of original series compared to any other reconstruction using any other n vectors (e.g. Fourier modes).

A similar technique in which the data vectors are formed from spatial patterns is often used in meteorology, where it is called Empirical Orthogonal Function (EOF) analysis (see e.g. Mo and Ghil (1987)). We can imagine a set of observations distributed in (phase) space. If we wished to form an orthonormal set of basis vectors that spanned the space, and the distribution were random, then there would be no preferred directions in which we should put our basis vectors. If, however, some underlying structure were present then observations would be clustered together in some regions and we would wish to place our basis vectors so that they pointed towards the more densely populated areas. The EOFs, or alternatively the eigenvectors from SSA, form an orthonormal basis for the space that are so directed to represent the most variable and important regions.

SSA has been found to offer advantages over the more traditional Fourier analysis in many contexts, not least in the analysis of noisy time series that are not statistically stationary e.g. time series that may contain long term trends or series that have a variance that changes with time (e.g. Allen *et al.* (1992)). It is for these reasons that we chose the technique to analyse the simulated and observed pressure data from VL2 which has a non-stationary variance due to the change from rather quiescent summer conditions, dominated by the diurnal cycle, to the larger amplitude oscillations associated with baroclinic waves in the winter season.

3 Analysis of Observed Viking Lander 2 Pressure Data

The SSA technique was applied to the observed VL2 pressure data shown in fig. 1. In order to remove the seasonal cycle, adjacent 10 day periods were averaged and a cubic spline was fitted to these values. This produced a smooth seasonal pressure curve, $p_s(t)$, that was then removed from the curve shown in fig. 1. In periods of missing data the pressure anomaly, $(p - p_s(t))$, was set to zero. Although this would be expected to cause spurious ringing in a conventional Fourier analysis, it is not a problem when using SSA as the zero pressure values contribute no variance to the time series and any abrupt changes in pressure would manifest themselves in higher order modes that only contribute below the 'noise floor'.

When using the SSA technique one is required to choose the window length in the time delay vector (M and k from eq. 2). If the timeseries under scrutiny contains oscillation patterns, it is desirable that window be long enough to capture the lowest frequency oscillation and the sample rate be frequent enough to capture the highest frequency oscillation (see e.g. Vautard *et al.* (1992)). In this study a window length of 14 Martian days, with $k = 5$ i.e. 5 samples per day for the VL2 data which has 25 bins per day, and $M = 70$, was found to give good results with the clearest signal separation, especially when comparing the eigenvectors from many different sources.

The first 8 eigenvectors from an analysis of the detrended VL2 series are shown in fig. 3. The structures are wave-like, with the eigenvectors forming pairs that have approximately the same shape but are displaced one quarter of a period out of phase. This indicates that each pair explains a recurrent oscillation pattern in the time series (Vautard *et al.* (1992))

We can assign an approximate period to the oscillation by finding the value of ω that maximises either

$$|\mathbf{e}_i \cdot \mathbf{s}| \tag{4}$$

or

$$|\mathbf{e}_i \cdot \mathbf{c}| \tag{5}$$

where

$$\mathbf{s} = \sin\left(\frac{2\pi\omega j}{M}\right)|_{j=1,M} \quad (6)$$

$$\mathbf{c} = \cos\left(\frac{2\pi\omega j}{M}\right)|_{j=1,M} \quad (7)$$

and $\mathbf{e}_i$ is the i'th eigenvector. This method exploits the fact that, like $\mathbf{s}$ and $\mathbf{c}$, the eigenvectors are either symmetric or antisymmetric about the mid-point of the window (in fact this only occurs in the limit of increasing time series length when the covariance matrix becomes Toeplitz, but it is a close approximation for all the eigenvectors presented here, see e.g. fig. 3).

Using this method the top four eigenvector pairs represent oscillations with periods 2.4, 7.2, 1.0 (the diurnal cycle) and 3.4 Martian days and account jointly for 18%, 15%, 13% and 11% of the series variance respectively. This should be compared to the frequency spectrum shown in fig. 2 and to those spectra given by Sharman and Ryan (1980) and Barnes (1980, 1981). In fig. 2 the spectral peaks that occur above the 95% confidence limit are at periods of 8.0, 7.1, 3.5, 3.4, 3.0, 2.3, 2.2 and 1.0 Martian days. The SSA technique thus picks out, in a clear and distinct way, the prominent modes of oscillation with periods close to those previously found by Sharman and Ryan (1980) and Barnes (1980, 1981).

The advantage of using the SSA technique over the Fourier analysis technique are twofold. Firstly SSA is data adaptive so that the decomposition is statistically optimal (see section 2), and secondly we can gain much more information about the time series by looking at its Principal Components (PCs). We note that any window, $\mathbf{x}_j$, in the time series can be expanded as a linear combination of the eigenvectors such that

$$\mathbf{x}_j = \sum_{i=1}^{M} p_{ij}\mathbf{e}_i, \quad (8)$$

where p_{ij} is the PC of the i^{th} eigenvector at position j in the time series. The PCs represent the amplitude of the eigenvector at a particular time. When the eigenvectors form an oscillatory pair we can take the square root of the sum of the squares of the two PCs to represent the amplitude of the oscillation at any time.

Figure 4 (a) shows the amplitudes of the 3.4 and 7.2 day oscillations during the first winter of measurements and fig. 4 (b) shows that amplitudes of the 2.4 and 7.2 day waves in the second year of measurements together with the corresponding detrended portions of the time series. There is a hint that the peaks in the amplitudes of the different oscillations are anti-correlated i.e when the amplitude of the low frequency wave is large the high frequency wave is small and *vice versa*. However, this interpretation maybe somewhat simplistic. There are certainly some interludes of mixed wave activity e.g. between days 340-390 and 920-980. Barnes (1980,1981) noted that low frequency modes are not dominant for long intervals, although there is a significant burst of low frequency activity after the first year dust storm (see fig. 4(a) VL2 Day 350-400). However, as we shall see, the interpretation of the curves in fig. 4 being anti-correlated is also suggested by the GCM simulations described below. This point is further discussed in section 7.

The diurnal cycle becomes particularly prominent between days 280 and 330, coincident with a major dust storm when dust optical depths were rose sharply to $\tau = 2 - 5$ (Pollack *et al.* (1979)). The presence of enhanced dust clearly increases the strength of the diurnal atmospheric heating, thus increasing the amplitude of the diurnal surface pressure cycle and also reducing the amplitude of the baroclinic wave activity. The model simulations of Barnes *et al.* (1993) suggested that baroclinic waves shift towards the north during high dust conditions thus reducing their amplitudes in midlatitudes.

Anticipating the model results described below, a possible interpretation of this analysis might be that the distribution of observed Martian baroclinic waves in frequency space is bimodal i.e. there are two distinct oscillating states corresponding to a low frequency (7.2 day) wave, and a high frequency (either 3.4 or 2.4 day) wave. Moreover the two states tend to be distinct in that they do not often appear simultaneously, but sporadically flip between states dominated by the low and high frequency oscillations on a time scale of approximately 50 days.

4 The Martian GCM

The Martian GCM (MGCM) used in this study can be thought of as consisting of two distinct components; the dynamical part that solves the adiabatic equations of motion of the atmosphere and the physical part that represents, for example, radiative heating and friction.

The dynamical part is based on the work of Hoskins and Simmons (1975). It solves the primitive equations of meteorology in spherical coordinates using the spectral method in the horizontal and finite-difference σ coordinates in the vertical (σ is equal to the pressure divided by the surface pressure). This part of the GCM has been used by Joshi *et al.* (1993,1995) and by Collins and

James (1995) in idealised studies of the Martian atmosphere.

The physical part of the GCM is closely based on that developed at the Laboratoire de Météorologie Dynamique (Hourdin *et al.* (1993)) and consists of a suite of parametrisation schemes that represent the effects of infrared radiative transfer in the 15 μm CO_2 band, radiative effects of dust in both the short and long waves, dry convection, boundary layer processes, surface heating, subsurface conduction of heat and the condensation and sublimation of CO_2 on the surface. Boundary conditions of surface thermal inertia and albedo are taken from the Consortium set blended with some additional information in the polar regions (kindly supplied by D. Paige of UCLA), whilst the surface orographic height was taken from the DTM data set (Wu (1978)). All data were interpolated and smoothed to the model resolution which was 48 longitude points by 24 latitude points. The dust visible optical depth was taken as constant over space and time and was set to 0.2, typical of low dust conditions (e.g. Pollack *et al.* (1979)). Results from simulations with higher dust optical depths will be reported in future publications.

A full description of the model and of its climatology is currently in preparation. One important feature of the model is described here as it is particularly relevant to the present study. The solar insolation can be prescribed in two ways. Either the insolation at any point on the planet can be made to vary diurnally (as it does in reality) or it can be set at a constant value, corresponding to the diurnal average, throughout the day. The latter option was initially used to reduce the number of times per day the radiative transfer tendencies needed to be calculated during the testing of the model. However, as we show below, this was found to have rather a profound affect on the baroclinic wave dynamics. We shall refer to integrations that include the diurnal variations in insolation as *diurnal cycle* runs, whilst the integrations that have diurnally-averaged insolation as *no diurnal cycle* runs.

5 Initial MGCM Experiments

The first task performed in running a Martian GCM is to establish the initial conditions, not only for the atmospheric part of the model but for the surface and sub-surface temperatures. As the soil model must respond to annual changes in insolation, the lowest model level in the soil takes several years to equilibrate. Thus a low vertical resolution version of the model with triangular truncation at total wavenumber 21 ($T21$), 5 equally spaced σ levels in the vertical and with no diurnal cycle, was first integrated for 20 Martian years. The final state of this run was then extrapolated in the vertical onto a grid with 10 equally spaced σ levels ranging from $\sigma = 0.95$, equivalent to an approximate height of 0.5 km, to $\sigma = 0.05$, equivalent to an approximate height of 30 km. This formed the initial conditions for the control integrations and for the subsequent sensitivity experiments. Other GCMs of the Martian atmosphere have used model tops somewhat higher than this (Barnes *et al.* (1993), Hourdin *et al.* (1993)) and we have included a some results from an integration in which the model top was placed at 87 km in section 6.

Two control experiments were performed, one in which no diurnal cycle in insolation was included and one in which the diurnal cycle was activated. Each integration was run for 9 Martian years, a total of 6021 Martian days, starting from $L_s = 0$ i.e. northern spring equinox. The first year of integration was ignored so as to ensure that all memory of the initial conditions was lost.

5.1 Simulated Viking Lander 2 Pressure: No Diurnal Cycle

Figure 5 shows the surface pressure from the VL2 position within the GCM for two typical years (5 and 7) from the integration with no diurnal cycle. The model has simulated the gross features of the annual cycle in pressure but did not capture the exact amplitude. This is largely due to a lack of 'tuning' of the albedo and emissivity in the polar regions but is also affected by the total atmospheric mass of the model and by the linear interpolation algorithm used to compute the VL2 pressure. Hourdin *et al.* (1994) have demonstrated the capabilities of the LMD GCM of producing a simulation of the annual pressure cycle which closely fits the observed VL2 measurements by separately tuning the albedo and emissivity at the Northern and Southern polar caps.

No oscillations in pressure occured during the northern hemisphere summer period (unless otherwise stated the seasons referred to shall be for the northern hemisphere) in this simulation, since there was no diurnal cycle in temperature and hence no diurnal tide (see e.g. Zurek (1988) and references therein). However, oscillations in pressure associated with baroclinic waves were simulated by the model during the late autumn, winter and early spring. The amplitude of these oscillations is generally similar to that seen in the Viking data (fig. 1), but the pattern in time is strikingly more regular. In year 5 a coherent baroclinic wave with a period of approximately 2.2 days persisted for the entire winter period, whilst in year 7 the 2.2 day wave occurred for only the first half of winter, and subsequently gave way to an approximate 5.5 day period wave in the latter half. Out of the 8 years of this simulation there were 2 years in which the high frequency oscillation persisted for the entire baroclinic wave season and 6 years when the winter started with the high frequency oscillation then flipped to a well defined lower frequency oscillation. The time of year at which the flip occurred was not constant but varied over an interval on the order of tens of days within each of the 6 years studied. The oscillations were in fact unrealistically regular compared to the observed data shown in fig. 1.

The SSA technique was applied to this simulated VL2 data. The surface pressure at the VL2 location was taken from the model 25 times per day (in order to provide easy comparison with the Viking data which was available at the same frequency). As for the actual VL2 data adjacent 10 day periods were averaged and a cubic spline was fitted to these values, Thus producing a smooth seasonal pressure curve that was then removed from the curves shown in fig. 5.

Figure 6 shows the top 4 eigenvectors computed from the last 8 years of the integration, using a window length of 14 Martian days. Eigenvectors 1 and 2 account for 47% of the variance between them while eigenvectors 3 and 4 explain 18% of the variance. The top 4 eigenvectors thus explain a sizable fraction (approximately 65%) of the time series variance.

Using the method described in section 3, equations (4-7), the periods of the oscillation patterns were determined as 5.5 and 2.2 days respectively. This can be compared with a traditional Fourier analysis shown in fig. 7. The two main spectral peaks are at periods of 5.3 and 2.2 days respectively and are present at the 95% confidence limit.

This behaviour is indicative of what is now recognised as a typical characteristic of many non-linear systems, in exhibiting two or more distinct and stable states (so-called 'multiple equilibria') which may coexist under otherwise identical imposed conditions. In the present context, the nearest analogue would seem to be the rotating, fluid annulus in the laboratory, which has been invoked elsewhere (e.g. Leovy 1985) as having a number of parallels with the quasi-regular baroclinic waves observed on Mars.

The annulus is well known (e.g. Hide & Mason 1975) to exhibit the co-existence of alternative regular wave states of differing wavenumber in certain regions of parameter space. Within this regime, transitions may be induced to occur between states by slowly varying the external control parameters (in this case the imposed temperature contrast ΔT and/or background rotation rate Ω), but in which the transitions exhibit a form of hysteresis, in the sense that the conditions under which a transition from one wavenumber state to another occurs may depend upon the direction in parameter space from which the transition is approached. In a context closer to that of our seasonally-varying GCM simulations, Buzyna et al. (1978) performed laboratory annulus experiments in which ΔT was varied cyclically within the regular wave regime. They found that transitions between different wavenumber states would occur sporadically within each 'seasonal cycle' of the variation of ΔT, in association with such hysteresis, indicating that the weak form of irregular interannual variability in the changeover of oscillation period (and indeed wavenumber, see section 5.3 below) within the winter season is a typical characteristic of a nonlinear baroclinic system.

5.2 Simulated Viking Lander 2 Pressure: With the Diurnal Cycle

In subsequence experiments the diurnal cycle was added to the model. It has been found from the data from both Viking landers that the diurnal cycle in pressure is large only during the summer season and during periods of high dust optical depths (see e.g. Tillman (1988)). The diurnal (and semi-diurnal) tide is generally weak during the baroclinic wave season and we would therefore expect the baroclinic waves to be largely unaffected by the diurnal tide. We would thus anticipate a pressure time series resembling that shown in fig. 5 but with a linearly superposed diurnal oscillation during summer (where the curve shows no oscillations in fig. 5).

Figure 8 shows the VL2 pressure sampled from years 5 and 7 of a 9 year integration of the GCM, with the diurnal cycle now switched on. The initial conditions for the integration were the same as that for the integration with no diurnal cycle. As anticipated above, the diurnal oscillation in pressure is evident as a thickening of the curve during the summer months. However the extremely regular baroclinic wave behaviour during the winter season has been replaced by a much more noisy signal that appears to be qualitatively similar to the observed VL2 data. The signal is clearly not consistent with a simple linear superposition of the previous highly regular baroclinic wave oscillations during winter and the diurnal oscillations dominant during summer.

The top 4 eigenvectors, computed from the last 8 years of this model integration using a window length of 14 Martian days, are shown in fig. 9 and again correspond to distinct oscillation pairs. The first two eigenvectors now account for 38% of the variance and the second two explain 11%, and the periods of oscillation represented by these eigenvectors are around 5.6 and 2.6 Martian days respectively. Eigenvectors 5 and 6 (not shown) form a pair which represents the diurnal tide and accounts for approximately 9% of the variance in total. Note the similarity now with the eigenvectors from the integration with no diurnal cycle. Although the pressure oscillations have, at first glance, become considerably less regular than in the case with no diurnal cycle, the underlying structure of the temporal patterns remain approximately the same. There are still essentially two baroclinic wave modes: a low frequency wave and a high frequency wave together now with the diurnal cycle.

In both the no diurnal and diurnal cycle cases however, the low frequency mode apparently accounts for more of the variance than the high frequency mode. This is in contrast to the VL2 observations themselves in which the high frequency mode is more prominent (see Barnes (1980,1981) and section 3). The fact that the analysis picks out two distinct frequencies of oscillation in each case is a good indication that the model is producing a reasonable qualitative simulation of the Martian atmosphere. Getting the ordering of the eigenvectors in the same sense as the observations and getting the frequencies to be more accurate would be a much more stringent quantitative test of a GCM. Indeed the simulations here have fixed dust distributions whereas it is known that the dust amount at both Viking sites varied considerably (Colburn *et al.* (1989)). Such factors like a more realistically seasonal variation of dust amount, realistic global dust distribution and accurate surface topography would probably be needed in order to obtain a more quantitatively correct simulation.

Figure 10 shows the root mean square combined amplitudes of the 2 eigenvector pairs during the winters of year 5 and 7, together with the corresponding detrended portions of the time series. Note that the curves for $\sqrt{(p_1)^2 + (p_2)^2}$ (solid line) and $\sqrt{(p_3)^2 + (p_4)^2}$ (dashed line) are typically anti-correlated i.e. when one is large the other is small and *vice versa.* The high and low frequency modes do not generally occur simultaneously except for short transition interludes. This behaviour is somewhat similar to that shown by the PC analysis of the observed Viking data (section 3, fig. 4) and it is suggested that the anti-correlation is caused by a competition between the low and high frequency modes that are present and separately stable in the no diurnal cycle runs. As we shall see in the next section this interpretation is supported by the fact that the high and low frequency modes have very similar spatial structures in both the diurnal and no diurnal cycle runs.

5.3 Spatial Structures

The spatial structures of the waves corresponding to the high and low frequency baroclinic components of the GCM simulations can be seen in figs. 11-14, which show polar stereographic maps of surface pressure anomaly over the life cycles of the high and low frequency waves from simulations both with and without the diurnal cycle. The high frequency wave shows a clear zonal wavenumber 2 structure whilst the low frequency wave is mainly zonal wavenumber 1. The waves, however, are not simple sinusoidal patterns, as their amplitudes are also spatially modulated by the surface orography.

It is of interest to compare fig. 11 with fig. 12 for the high frequency wavenumber 2 modes and fig. 13 with fig. 14 for the low frequency wavenumber 1 mode. The spatial structures show very similar features between the simulations with the diurnal cycle and those without. As the results using the SSA technique suggested, the waves are essentially the same in the two integrations.

The wavenumbers seen here are somewhat at odds with those seen in other studies. Barnes (1980,1981) associated zonal wavenumbers 1-2 with low frequency oscillations and wavenumbers 3-4 with high frequency oscillations in the measured VL2 data. However the estimates were by no means unique, since observations taken at one point could be consistent with a number of different wavenumbers and phase speeds. In modelling studies using the NASA Ames GCM Barnes *et al.* (1993) found that wavenumbers 1-2 had periods in the range 3-8 days whilst wavenumbers 3-4 had periods in the 1-3 day range (see e.g. fig. 8(a) of their paper). Also Collins and James (1995) found wavenumbers 3 and 4 using a GCM with simplified physical parametrisations.

Quite why the wavenumbers are generally smaller in our model, compared with those found previously, is unclear. The dynamical solver used here is the same as that used by Collins and James (1995), although the physical parametrisation schemes are much more sophisticated. In particular the the surface topography is parametrised in the GCM but was absent in the work of Collins and James (1995). The topography contains large variations on the zonal wavenumber 1 and 2 scales and it is possible that interactions with these components and the transient baroclinic waves may bias the GCM toward forming lower wavenumber transients. Alternatively, differences in the mean state of the models may be important. In the NASA Ames model also, wavenumbers 3-4 appear to have quite large amplitude whereas in this study they do not. Differences in the mean states of the atmosphere between the two models may again produce such an effect. However, a quick examination of our model climatology shows no major differences to that of the Ames model. Differences in the models' dynamical formulations or physical parametrisation schemes may be important but would require a detailed study.

The two simulations with the Oxford MGCM indicate a mechanism for the mode flipping. In the absence of the diurnal cycle the baroclinic waves are remarkably, and quite unrealistically, regular. Mode flipping from the high to low frequency wave occurs at most once a season and sometimes not at all. When the diurnal cycle is added, however, exchanges between the two modes happen much more often so that, for instance, in year 7, 4 transitions can be discerned. The thermal tide must therefore play a crucial role in forcing the mode flipping between two otherwise coexisting stable and intransitive states . This hypothesis is further discussed in section 7.

6 Other Simulations

The two simulations described in the previous section, and in particular the integration with the diurnal cycle, seems to agree well with the observations. It is well known, however, that the circulations produced by GCMs can often be sensitive to many factors, such as the algorithms used in the parametrisation schemes or the specification of boundary conditions. For this reason we have performed some sensitivity studies using the MGCM, and also using the LMD Martian GCM.

The LMD Martian GCM comprises a dynamical solver consisting of the finite difference (leapfrog) scheme originally described by Sadourny and Laval (1984), and the physical parametrisation package described by Hourdin *et al.* (1994) that is also used in the Oxford MGCM (albeit with some minor modifications). This model was run with a horizontal resolution of 32 points in longitude and 24 points in latitude and with a vertical resolution of 15 unequally spaced σ levels that extended from a height of approximately 85 m above to the surface to approximately 69 km at the model top. The orography was taken from the Consortium data set, in contrast to the Oxford MGCM which uses the DTM data set. A uniform dust visible optical depth of 0.2 was used as in the initial Oxford MGCM experiments described in the previous section.

Figure 15 shows two time series of pressure at the VL2 location, each taken from 2 years of simulations using the LMD GCM. In fig. 15 (a) the diurnal cycle was switched off whilst in fig. 15 (b) it was included. The gross features of the time series i.e. the seasonal cycle and the amplitude of the diurnal and baroclinic waves show good agreement with the observations and with the Oxford MGCM. The only significant difference is that the low frequency mode appears to be less frequently seen in the LMD model than in the Oxford GCM, both with and without the diurnal cycle. It is noticeable that in the simulation with no diurnal cycle (fig. 15 (a)) the baroclinic waves start off being very regular in time, much like those found in the Oxford model with no diurnal cycle (fig. 5). Rather than staying regular, or flipping to a longer period very regular oscillation around midwinter, however, the waves become less coherent just before the seasonal peak in surface pressure. Some lower frequency waves can be discerned by eye, interspersed with high frequency oscillations. In the simulation with the diurnal cycle (fig. 15 (b)), however, the baroclinic waves appear to be much less regular, resembling those seen in the observations and in the Oxford GCM with the diurnal cycle (fig. 8).

The top four eigenvectors computed using the SSA technique on the 5 years of simulation of the LMD GCM, again with a window length of 14 days and with the diurnal cycle included, are shown in fig. 16. The first two eigenvectors now explain 27% of the variance and the second two account for 15% of the variance. Note how the order of the eigenvectors in this simulation is reversed compared to those shown in figs. 6 and 9 i.e. the high frequency oscillation, in this case with a period of 2.4 days, is more prominent than the low frequency 6.7 day wave. This situation is much more like that seen in the analysis of the observed VL2 data (fig. 3). In the Oxford model the low frequency component was more prominent. However the modes are broadly similar in behaviour and structure and indicate again a bimodal distribution of baroclinic wave frequencies.

The spatial modes of the LMD model are shown in figure 17. As in the Oxford GCM the low frequency oscillation is caused by a zonal wavenumber 1 mode and the high frequency oscillation is caused by a zonal wavenumber 2 mode. Hence the LMD grid point model and the Oxford spectral model produce very similar baroclinic modes but the relative occurrence of the modes is different, with the LMD model favouring the wave 2 mode as the most prominent pattern and the Oxford model favouring the wave 1 mode.

Some further sensitivity experiments were also performed with the Oxford GCM. In particular two 9 year simulations, one with the diurnal cycle and the other without, were performed using the Consortium orography data set. The eigenvectors from the SSA technique are not presented here as they are very similar to those from the control simulations that used the DTM orography. The analysis again picked out two modes of oscillation; a low frequency 5-6 day wave and a high frequency 2-3 day wave. Examination of the spatial fields showed that waves of zonal wavenumbers 1 and 2, respectively, were responsible for the oscillations. The model baroclinic wave behaviour seems quite insensitive to the choice of either the DTM or Consortium orography data sets.

Other GCMs have had their model tops places somewhat higher than that used in this paper. To address this problem we performed a one year simulation using a horizontal resolution of $T21$ but with 20 σ levels in the vertical. The spacing between the levels in physical height was chosen so that they were closer together near the ground than at upper levels, with the top most level placed at an approximate height of 87 km. The SSA technique was applied to the 1 year of simulatated VL2 pressure detrended as before and a selection the eigenvectors are shown in figure 18. Eigenvectors 1 and 2 represent an oscillation with a period of 5.4 days while eigenvectors 5 and 6 represent an oscillation with a period of 2.8 days. The period of oscillation represented by eigenvectors 3 and 4 is 1.6 days, being somewhat shorter than the high frequency 2-3 day periods found in the 10 level integrations. It may be the case that the appearance of the shorter period oscillation is just a quirk of performing the analysis on one year of simulated VL2 pressure and indeed some of the lower order eigenvectors from the 10 level integrations do represent oscillations of similar periods. Nevertheless the principle component behaviour still shows the same anti-correlation in the amplitudes of the modes. The bimodality is a robust feature of all the low dust simulations we have examined.

7 Discussion/Conclusions

The results presented above have shown that the frequency distribution of the highly regular baroclinic wave activity in the Martian atmosphere is nearly bimodal. Singular systems analysis of surface pressure data taken from the Viking Lander 2 mission and of data taken from several Martian GCM simulations give very similar eigenvector patterns that represent respectively a low frequency 5-7 day oscillation and a high frequency 2-3 day oscillation. Moreover we have shown the amplitudes of the two oscillations are typically anti-correlated i.e. when one is large the other is usually small and *vice versa*.

The regular nature of the GCM baroclinic waves is also evident in the spatial fields. The low frequency wave is seen to be largely made up of a zonal wavenumber 1 disturbance, whilst the high frequency mode comprises a zonal wavenumber 2 wave (figs. 11-14). The waves are not simple sinusoidal modes, however, and their surface amplitude is significantly modulated by the orography (cf also Collins *et al.* (1994), their fig. 2, which shows longitude-time plots of surface pressure anomaly).

The apparent bimodal character of the baroclinic wave regimes in the GCM simulations without the diurnal forcing is also strongly suggestive of a system with intransitive multiple equilibria or 'basins of attraction'. Such coexistence of two or more separately stable states at a given point in parameter space is well known in other areas of dynamical meteorology (e.g. Charney & DeVore (1979)), and in baroclinic wave flows in the laboratory rotating annulus (Hide & Mason (1975)) subject to steady boundary conditions. In the latter case, two or more steady, regular wave states may occur at a given point in parameter space, the particular state observed in any one experiment depending upon the route followed to approach it. This situation was interpreted by Moroz & Holmes (1984) as an unfolding of a co-dimension 2 point at which two different baroclinic wavenumber flows simultaneously become linearly unstable. The observed transition from one wavenumber state to another during the seasonal cycle in the MGCM simulations is then strongly hysteretic, much as observed in laboratory experiments in which the thermal boundary conditions are varied cyclically on time scales comparable with, or longer than, the growth time scale of the instability (Buzyna *et al* (1978)).

The addition of the diurnal cycle in the MGCM simulations appears to act as a perturbation to this bistable system, triggering erratic flips between the two otherwise stable states provided the frequency of the forcing is not commensurate with that of either baroclinic wave state. The previously distinct attracting states corresponding to the two coexisting stable wave regimes are thus connected as a result of the external perturbation, and form a more complex, and possibly chaotic, merged attractor.

Similar forms of 'attractor merging' through external perturbations have been studied, for example, in the context of noise-induced chaos, found e.g. in experiments on Josephson junctions (Iansiti *et al.* (1985); Sommerer *et al.* (1991); Gaveau *et al.* (1992); Bulsara *et al.* (1990); Hamm *et al.* (1994)), and in periodically-forced forms of other kinds of nonlinear oscillator (e.g. the double-well Duffing oscillator, Moon (1987)). A system is particularly sensitive to external perturbations if two initially distinct attractors are nearby in phase space, if the attractor leads the trajectory of the system close to its basin boundary, or if the basin boundary itself is only weakly repelling. These conditions are often found close to bifurcations, where spontaneous transitions would occur without perturbations. It is of interest to remark that a similar scenario, in which intermittent long time scale variability is associated with switching between a small number of metastable states or 'weather regimes', has been suggested (a) in the context of the Earth's weather regimes (Plaut & Vautard (1994)), where baroclinic transients play the role of a noisy perturbation, and (b) in relation to the El Niño-Southern Oscillation (Jin *et al.* (1994)) for which the annual seasonal cycle provides the perturbation. In the latter case, an intricate set of frequency locking between the ENSO and and the annual cycle may be observed in the form of a 'devils staircase'.

A further complication arises in the present system because the diurnal tide, with a principal zonal wavenumber 1 structure, is *spatially* resonant with one of the baroclinic wave states (though has a very different temporal frequency). Such a spatial resonance renders a theoretical analysis of this problem more complex, owing to the potentially strong nonlinear interactions between resonant modes compared with the non-resonant case, and which may modify significantly the bifurcation structures (cf Jones & Proctor (1985)). Also the diurnal tide may itself excite other resonant modes, such as Kelvin waves (Zurek (1988)) which may, in turn, interact with the baroclinic waves. To our knowledge the complete unfolding of the generic form of the 1:1 spatially resonant mode interaction, corresponding to the thermal tide/baroclinic wave interaction here, has not so far been solved in detail.

Despite these uncertainties, however, we may conclude that nonlinear interactions between the baroclinic waves and the thermal tide on Mars must be important in determining the degree of spatial and temporal irregularity during the northern baroclinic wave season. Even though the diurnal cycle has only a small amplitude at the time of the baroclinic wave season, the resultant response consists of much more than a simple linear combination of the discrete frequencies from the contributing baroclinic and tidal modes, and may even produce a chaotic response from an otherwise quasi periodic system (though we have not proved, so far as one can, that the perturbed system is indeed chaotic in a low dimensional sense).

Many questions are raised by this work. For instance how does the amplitude of the diurnal cycle affect the frequency of flipping? This is quite a difficult sensitivity experiment to perform in a full GCM as the tidal amplitude is dependent on many aspects of the planet, for instance the dust loading and the surface thermal inertia, which also affect directly the baroclinic waves. Also the seasonal cycle in pressure complicates matters. It may be possible to perform experiments in which the seasonal date and the boundary conditions i.e. surface temperature and ice cover are held fixed and diurnal cycle of surface temperature is added to stimulate the thermal tide. This assumes that diurnal heating and cooling due to the radiative effects of dust and CO_2 are negligible.

Other questions involve the sensitivity of the GCM integrations and their baroclinic wave activity to such factors as dust loading, horizontal and vertical resolution, the inclusion of more parametrisation schemes such as gravity wave drag, etc. All these are areas that we shall be exploring in the future.

8 References

Allen, M.R., P.L. Read, L.A. Smith 1992. Temperature oscillations. *Nature,* **359**, 679.

Barnes, J.R. 1980. Time spectral analysis of midlatitude disturbances in the Martian atmosphere. *J. Atmos. Sci.,* **37**, 2002-2015.

Barnes, J.R. 1981. Midlatitude disturbances in the Martian atmosphere: A second Mars year. *J. Atmos. Sci.,* **38**, 225-234.

Barnes, J.R. 1984. Linear baroclinic instability in the Martian atmosphere. *J. Atmos. Sci.,* **41**, 1536-1550.

Barnes, J.R. 1986. Finite-amplitude behaviour of a single baroclinic wave with multiple vertical modes: Effects of thermal damping. *J. Atmos. Sci.,* **43**, 58-71.

Barnes, J.R., J.B. Pollack, R.M. Haberle, R.W. Zurek, C.B. Leovy, H. Lee and J. Schaeffer 1993. Mars atmospheric dynamics as simulated by the NASA Ames general circulation model: II Transient baroclinic eddies. *J. Geophys. Res.*, **98**, 3125-3148.

Broomhead, D.S. and G. King 1986. Extracting qualitative dynamics from experimental data. *Physica D*, **20**, 217-236.

Bulsara, A.R., W.C. Schieve and E.W. Jacobs 1990. Homoclinic chaos system perturbed by weak Langevain noise, *Phys. Rev.*, **41**, 668-681.

Buzyna, G., R.L. Pfeffer and R. Kung 1978. Cyclic variations of the imposed temperature contrast in a thermally driven rotating annulus of fluid. *J. Atmos. Sci.*, **35**, 859-881.

Chamberlain, T.E., H.L. Cole, R.G. Dutton, G.C. Greene and J.E. Tillman 1976. Atmospheric measurements on Mars: The Viking meteorology experiment. *Bull. Amer. Meteorl. Soc.*, **57**, 1094-1104.

Charney, J.G. and J.G. DeVore 1979. Multiple flow equilibria in the atmosphere and blocking.*J. Atmos. Sci.*, **36**, 1205-1216.

Colburn, D., J.B. Pollack and R.M. Haberle 1989. Diurnal variations in dust optical depth at Mars. *Icarus*, **79**, 159-189.

Collins, M. and I.N. James 1995. Regular baroclinic transient waves in a simplified global circulation model of the Martian atmosphere. *J. Geophys. Res.*, **100**, E7, 14421-14432.

Collins, M., S.R. Lewis and P.L. Read 1995. Regular and irregular baroclinic waves in a Martian general circulation model: A role for diurnal forcing? *Adv. Space Res.* **Vol. 16 No. 6**, 3-7.

Fraedrich, K. 1986. Estimating the dimensions of weather and climate attractors. *J. Atmos. Sci.*, **43**, 331-344.

Gadian, A.M. 1978. The dynamics of and the heat transport by baroclinic eddies and large scale stationary topographically forced long waves in the Martian atmosphere. *Icarus*, **33**, 454-465.

Gaveau, B., E. Gudowsku-Nowal, R. Kapral and M. Moreau 1992. Stochastic transitions between a limit cycle and a fixed point. *Physica A*, **188**, 443-451.

Hamm, A., T. Tél and R. Graham 1994. Noise induced attractor explosions near tangent bifurcations. *Phys. Lett. A*, **185**, 313-320.

Hartmann, D. 1974. Time spectral analysis of midlatitude disturbances. *Mon. Wea. Rev.*, **102**, 348-362, Corrigendum 541-542.

Hess, S.L. 1950, Some aspects of the meteorology of Mars. *J. Meteorol.*, **7**, 1-13.

Hide, R. and P.J. Mason 1975. Sloping convection in a rotating fluid. *Adv. in Phys.*, **24**, 47-100.

Hoskins, B.J. & A.J. Simmons 1975. A Multi-Layer Spectral Model and the Semi-Implicit Method. *Quart. J. R. Met. Soc.*, **109**, 771-783.

Hourdin, F., P. Le Van, F. Forget and O. Talagrand 1993. Meteorological Variability and the Annual Surface Pressure Cycle on Mars. *J. Atmos. Sci.*, **50**, 3625-3640.

Hourdin, F., F. Forget and O. Talagrand 1995. The sensitivity of the Martian surface pressure and atmospheric mass budget to various parameters: a comparison between numerical simulations and Viking observations. *Accepted for publication in J. Geophys. Res.*

Iansiti, M. Qing Hu, R.M. Westervelt and M. Tinkham 1985. Noise and chaos in a fractal basin boundary regime of a Josephson Junction. *Phys. Rev. Lett.*, **55:7**, 746-749.

James, I.N. and P.M. James 1992. Spatial structure of ultra-low-frequency variability of the flow in simple atmospheric circulation model. *Quart. J. R. Met. Soc.*, **118**, 1211-1234.

Jin, F.F., J.D. Neelin and M. Ghil 1994. El Niño on the devil's staircase: Annual subharmonic steps to chaos. *Science*, **269**, 70-72.

Jones, C.A. and M.R.E. Proctor 1987. Strong spatial resonance and travelling waves in Benard convection. Phys. Lett. A, **121:5**, 224-228.

Joshi, M.M., S.R. Lewis, P.L. Read and D.C. Catling 1994. Western boundary currents in the atmosphere of Mars. *Nature*, **367**, 548-551.

Leovy, C.B. 1969. Mars: Theoretical aspects of meteorology. *Appl. Opt.*, **8**, 1279-1286.

Leovy, C.B., Y. Mintz 1969. Numerical simulations of the weather and climate of Mars. *J. Atmos. Sci.*, **26**, 1169-1190.

Leovy, C.B. 1985. The general circulation of Mars: Models and observations. *Adv. Geophys.*, **28a**, 327-346.

Mo, K.C., and M. Ghil 1987. Statistics and dynamics of persistent anomalies. *J. Atmos. Sci.*, **55**, 877-901.

Moon, F.C. 1979. *Chaotic Vibrations.* John Wiley & Sons.

Moroz, I.M. and P. Holmes 1984. Double Hopf bifurcation and quasi-periodic flow in a model for baroclinic instability. *J. Atmos. Sci.*, **41**, 3147-3159.

Plaut, G. and R. Vautard 1994. Spells of low-frequency oscillations and weather regimes in the northern hemisphere. *J. Atmos. Sci.*, **51**, 210-236.

Pollack, J.B., D.S. Colburn, F.M. Flasar, R. Khan, C.E. Carlston and D.C. Pidek 1979. Properties and effects of dust particles suspended in the Martian atmosphere. *J. Geophys. Res.*, **84**, 2929-2945.

Pollack, J.B., C.B. Leovy, P.W. Greiman and Y.Mintz 1981. A Martian general circulation model with large topography. *J. Atmos. Sci.*, **38**, 3-29.

Sadourny, R. and K. Laval 1984. January and July performance of the LMD general circulation model. In *New Perspectives in Climate Modelling*, A. Berger and C. Nicolis eds., 173-197 Elsevier.

Sharman, R.D. and J.A. Ryan 1980. Mars atmospheric pressure periodicities from Viking observations. *J. Atmos. Sci.*, **37**, 1994-2001.

Sommerer, J.C., W.L. Ditto, C. Grebogi, E. Ott and M.L. Spano 1991. Experimental confirmation of the scaling theory for noise-induced crises. *Phys. Rev. Letts.*, **66**, 1947-1950.

Tillman, J.E. 1988. Mars global atmospheric oscillations: Annually synchronised, transient normal mode oscillations and the triggering of global dust storms. *J. Geophys. Res.*, **84**, 2947-2955.

Vautard, R., P. Yiou and M. Ghil 1992. Singular-spectrum analysis: A toolkit for short, noisy chaotic signals. *Physica D*, **58**, 95-125.

Wu, S.S.C. 1978. Mars synthetic topography mapping. *Icarus*, **33**, 417-440.

Zurek, R.W. 1988. Free and forced modes in the Martian atmosphere. *J. Geophys. Res.*, **93**, 652-670.

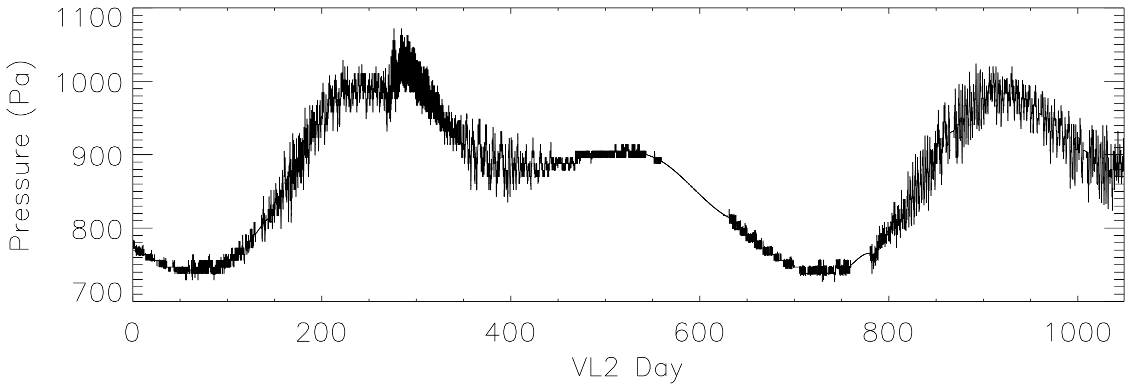

Figure 1: Pressure from Viking Lander 2 for the entire mission. Missing data values have been fitted with a cubic spline.

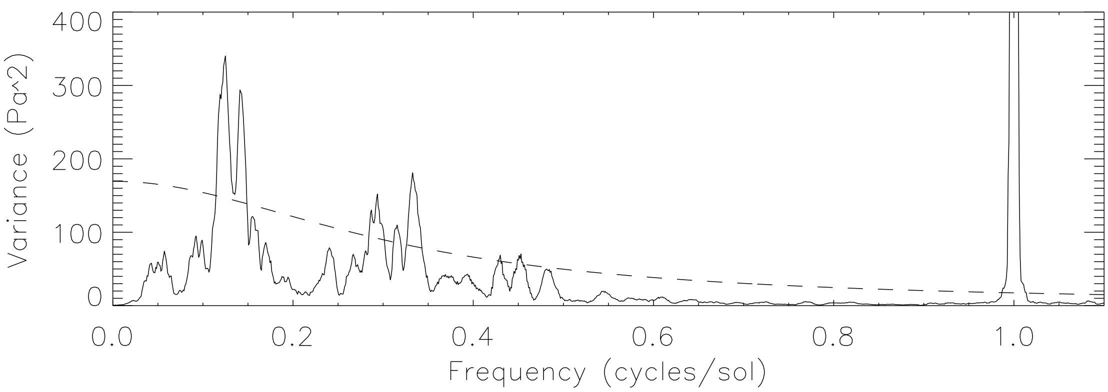

Figure 2: Frequency spectrum (solid line) of the detrended version of the data shown in fig. 1. The dashed line indicates the line above which the spectral peaks must extend in order to be 95% confident that they are not red noise.

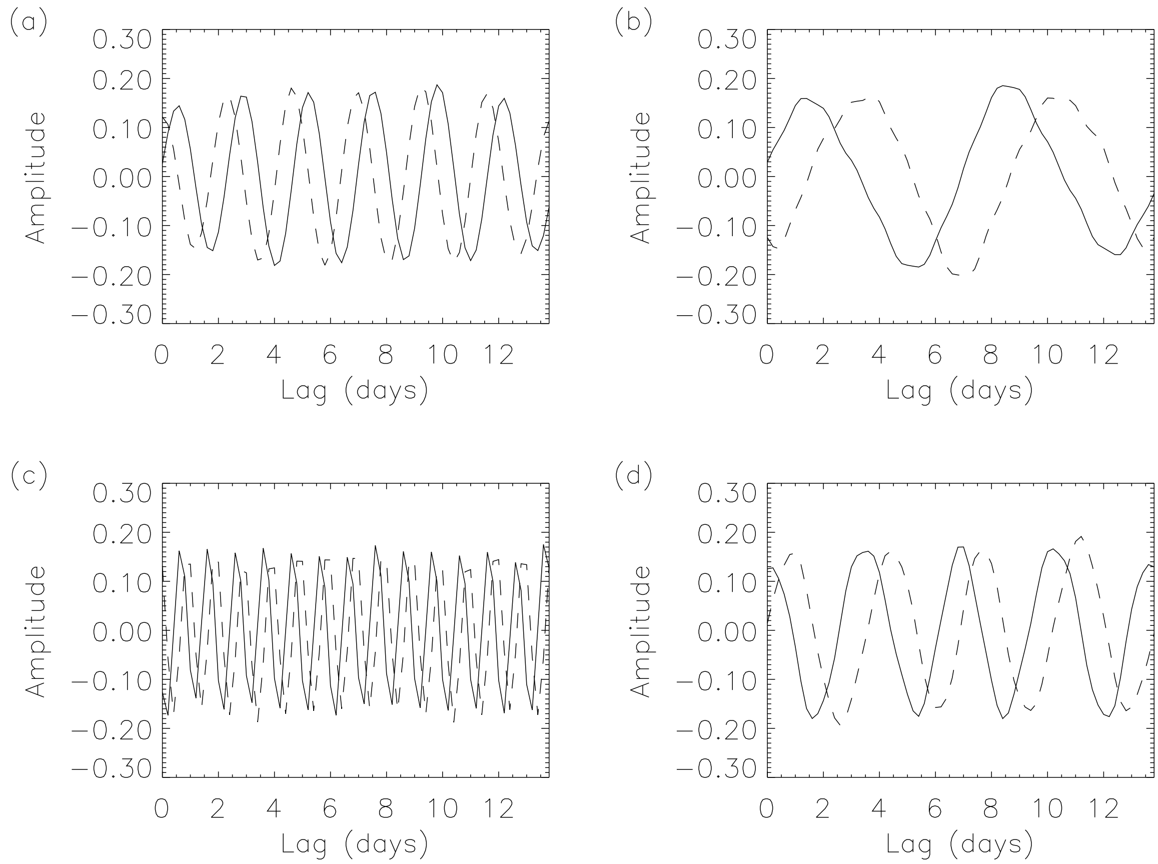

Figure 3: The top 8 eigenvectors from the SSA analysis of the Viking data. (a) Eigenvector 1 (solid line), Eigenvector 2 (dashed line). (b) Eigenvector 3 (solid line), Eigenvector 4 (dashed line). (c) Eigenvector 5 (solid line), Eigenvector 6 (dashed line). (d) Eigenvector 7 (solid line), Eigenvector 8 (dashed line).

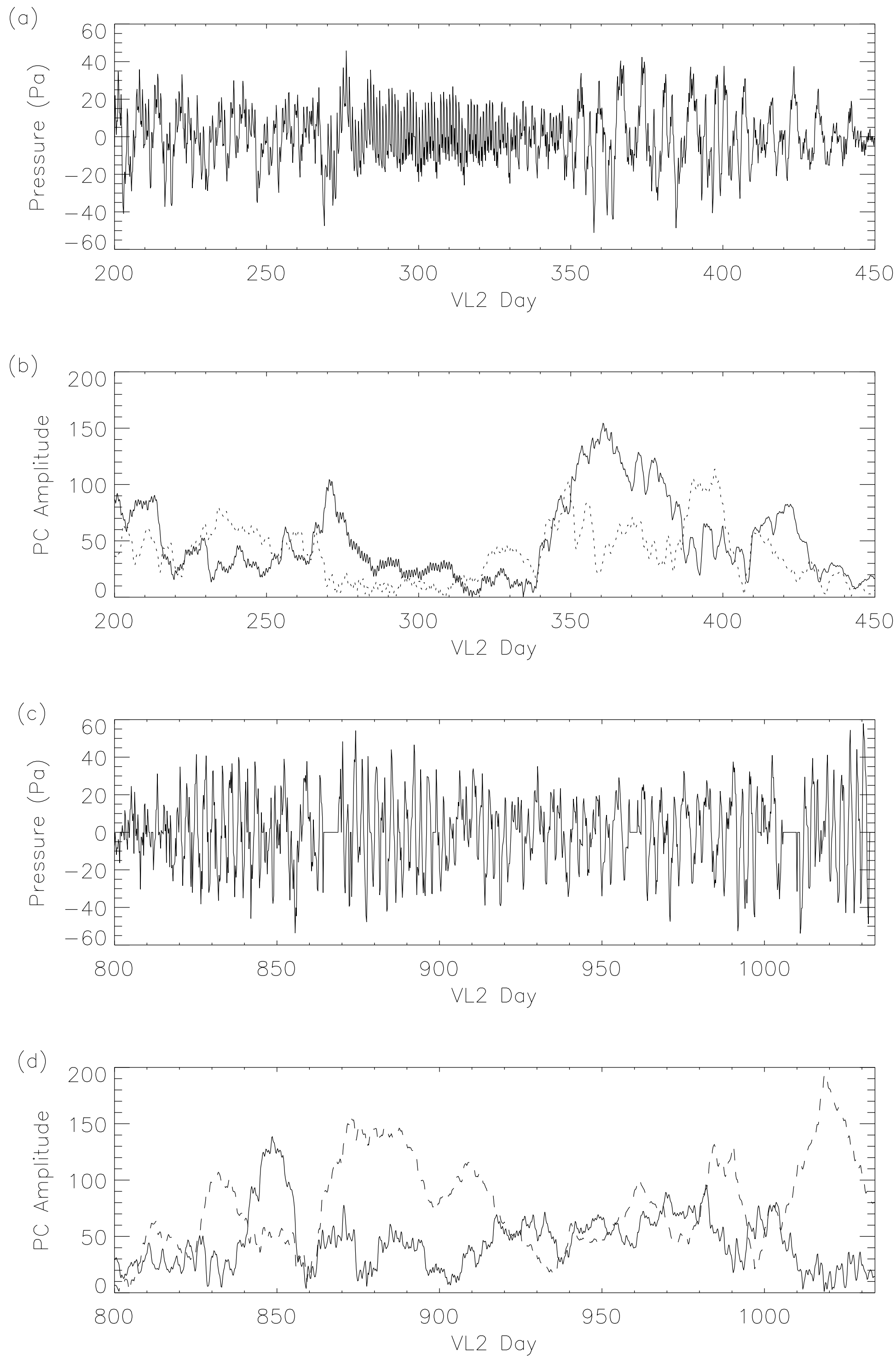

Figure 4:

(a) and (c) Detrended portions of the VL2 pressure curve shown in fig. 1 and root mean square principle component amplitudes for various eigenvectors, (b) $\sqrt{p_3^2+p_4^2}$ (solid line) and $\sqrt{p_7^2+p_8^2}$ (dotted line) during the first winter of observations, (d) $\sqrt{p_1^2+p_2^2}$ (dashed line) and $\sqrt{p_3^2+p_4^2}$ (solid line) during the second winter of observations. Note how the peaks and troughs are anti-correlated.

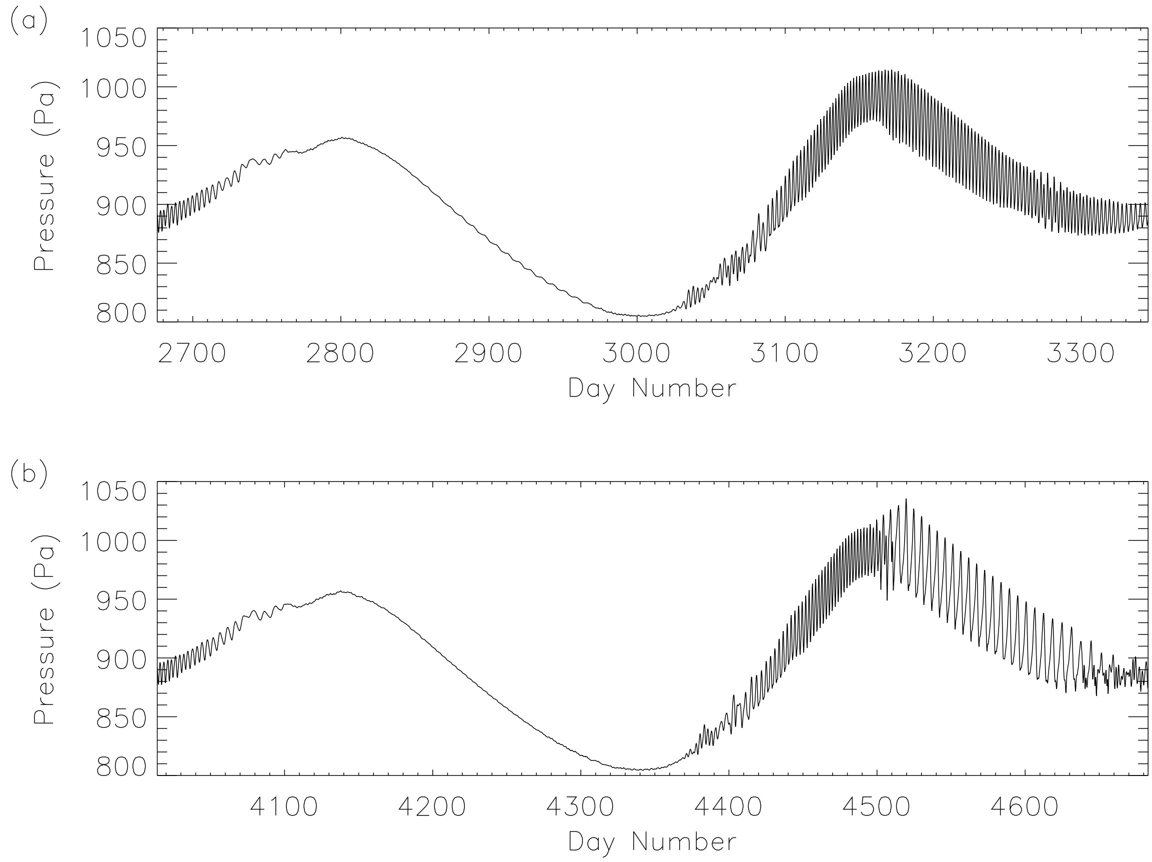

Figure 5: Simulated VL2 pressure from the GCM simulation with no diurnal cycle. (a) Year 5 and (b) Year 7.

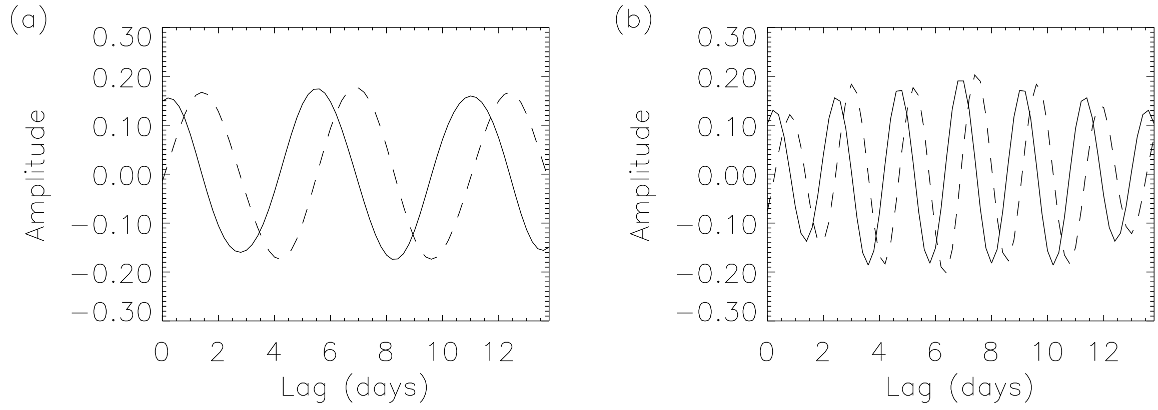

Figure 6:

The top 4 eigenvectors computed from the detrended version of the data from the integration with no diurnal cycle (fig. 5). (a) Eigenvector 1 (solid line), Eigenvector 2 (dashed line). (b) Eigenvector 3 (solid line), Eigenvector 4 (dashed line). A window length of 14 days was used.

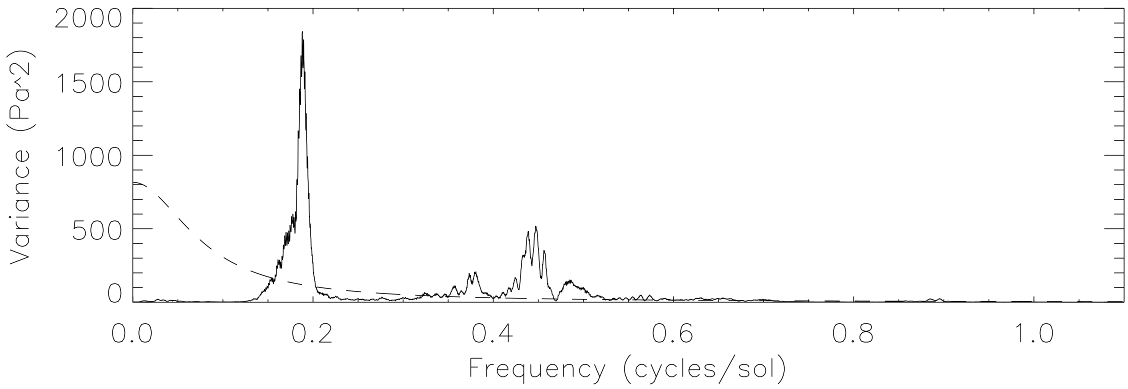

Figure 7: Frequency spectrum (solid line) of the detrended version of the data shown in fig. 5. The dashed line indicates the line above which the spectral peaks must extend in order to be 95% confident that they are not red noise.

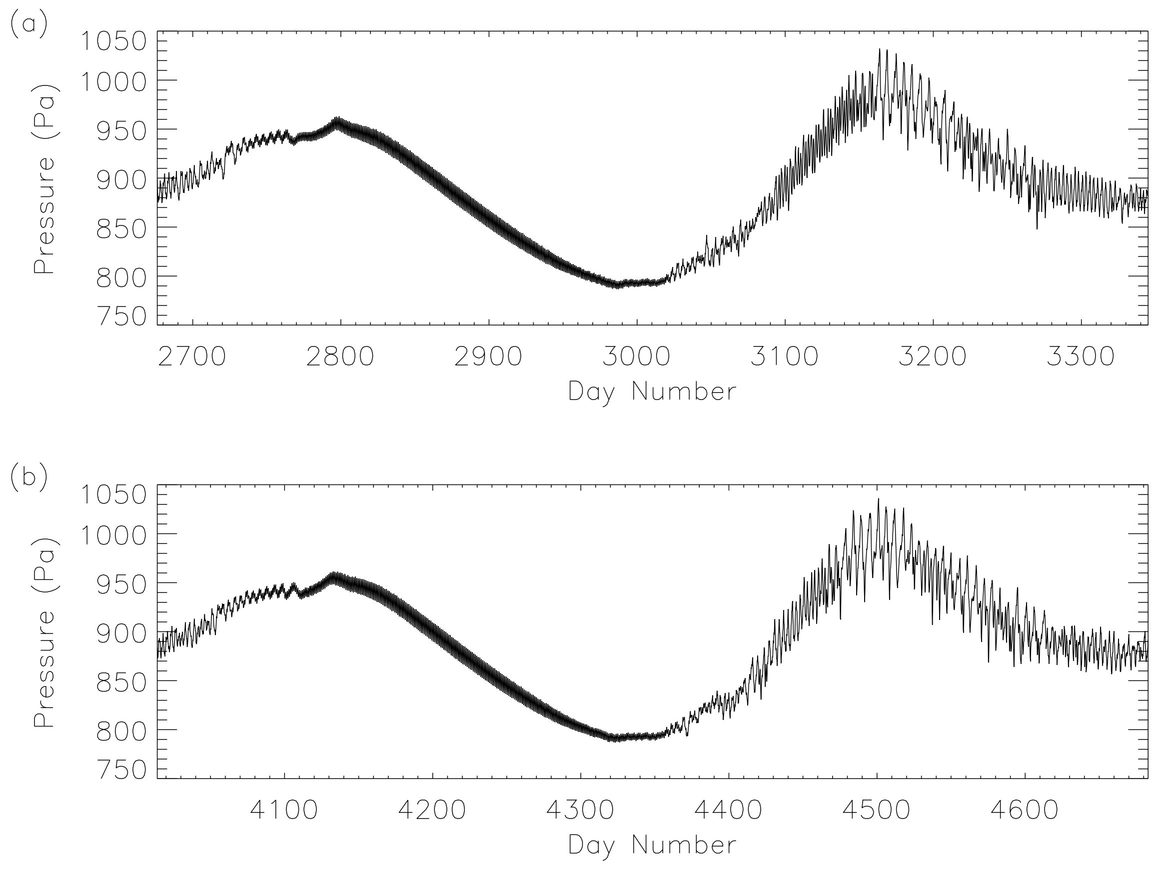

Figure 8: Simulated VL2 pressure taken from the GCM simulation with the diurnal cycle. (a) Year 5 and (b) Year 7.

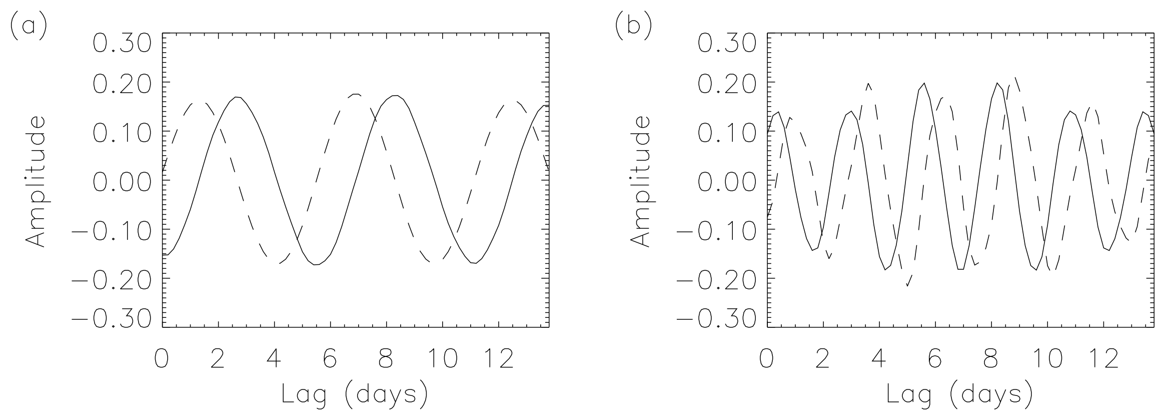

Figure 9: The top 4 eigenvectors computed from the detrended version of the data from the integration with the diurnal cycle (fig. 8). (a) Eigenvector 1 (solid line), Eigenvector 2 (dashed line). (b) Eigenvector 3 (solid line), Eigenvector 4 (dashed line). A window length of 14 days was used.

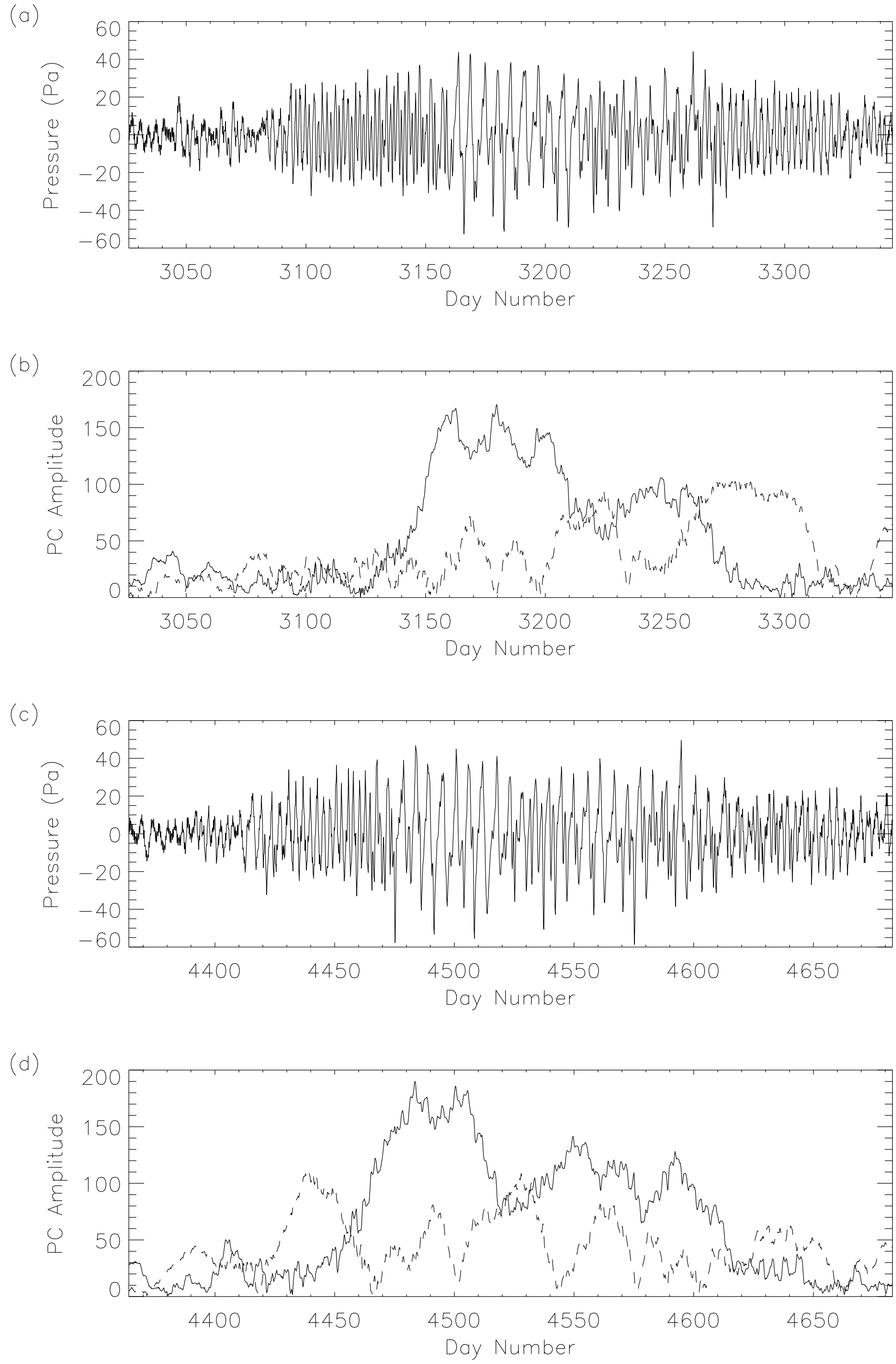

Figure 10:

Detrended pressure time series from the integration with the diurnal cycle (a) the winter of year 5 and (c) the winter of year 7, and root mean square amplitudes of the PCs of the top 4 eigenvectors $\sqrt{(p_1)^2+(p_2)^2}$ (solid line) and $\sqrt{(p_3)^2+(p_4)^2}$ (dashed line), for (b) the winter of year 5 and (d) the winter of year 7.

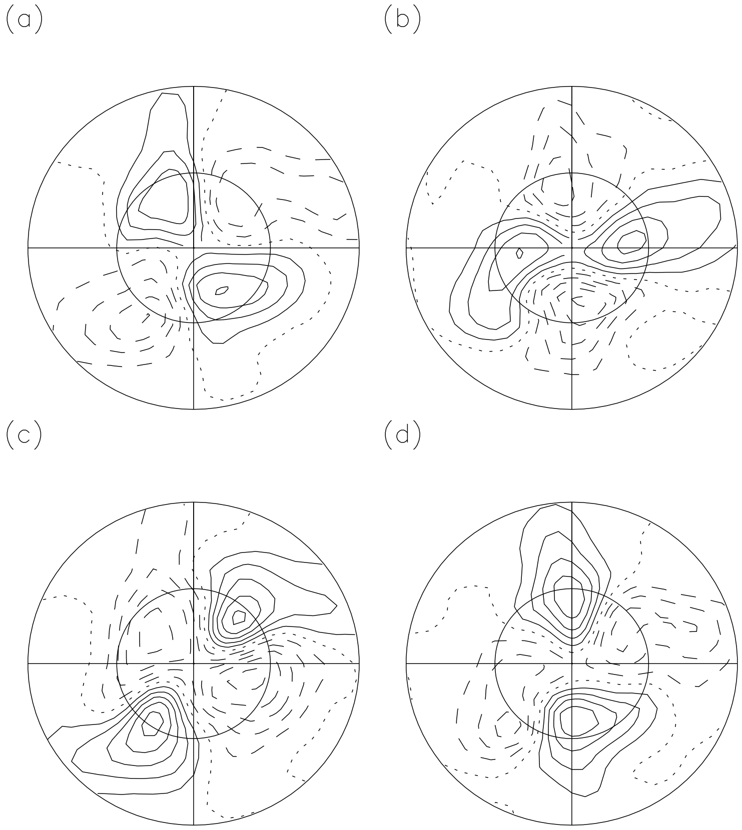

Figure 11: (a)-(d) Snapshots of transient surface pressure anomaly over the life cycle of a high frequency 2.2 day wave, from the integration with no diurnal cycle. The plots are shown every 0.6 days. A northern hemisphere polar stereographic projection has been used with the north pole at the centre, the outermost circle at 30°N and the inner circle at 60°N. Lines of longitude are drawn every 90° and the 0° longitude is lower line on each plot. The units are Pascals and the contour interval is 10 Pa. Positive contours are drawn solid, negative dashed and the zero contour is draw dotted.

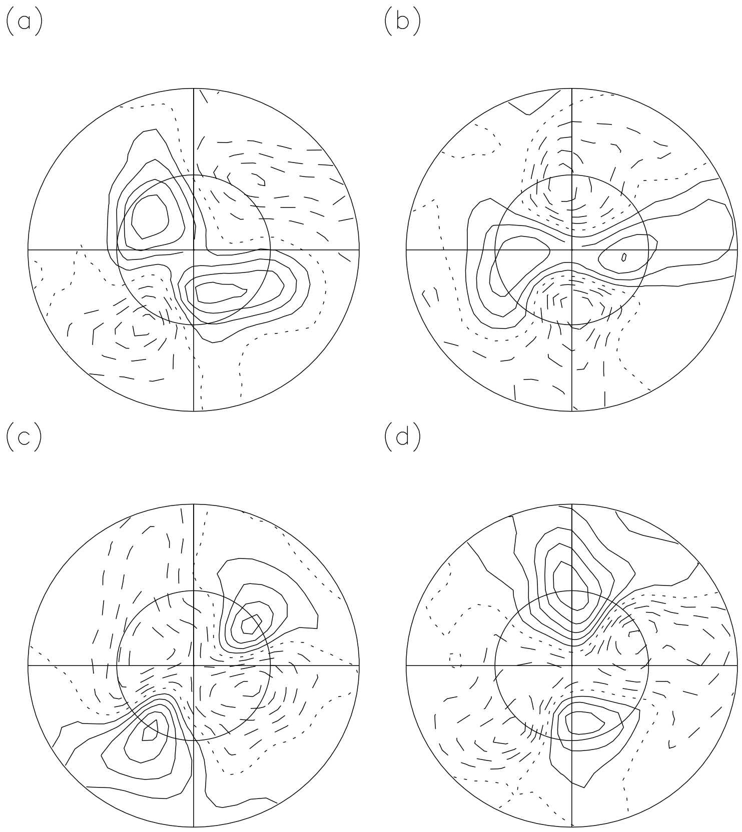

Figure 12: As in fig. 11 but for a life cycle of the high frequency wave from the integration which includes the diurnal cycle.

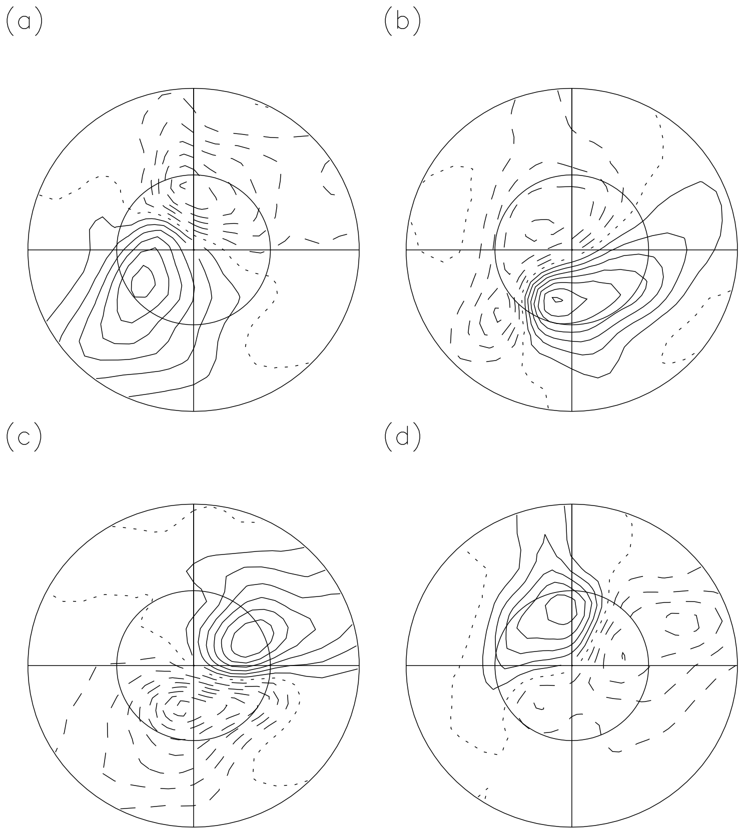

Figure 13: As in fig. 11 but for a life cycle of the low frequency 5.5 day wave from the integration with no diurnal cycle. In this case the plots are every 1.4 days.

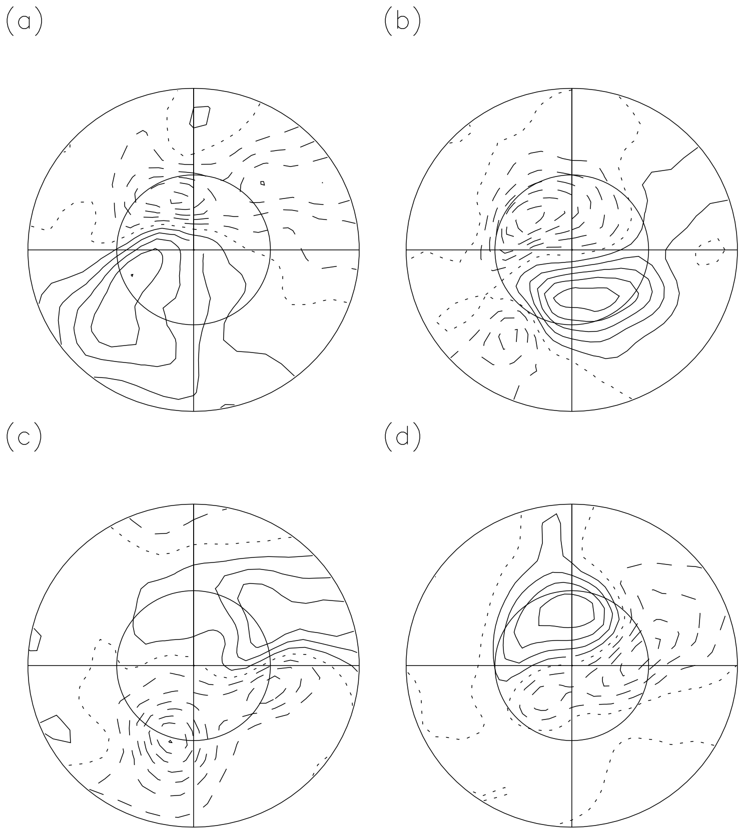

Figure 14: As in fig. 13 but for a life cycle of the low frequency wave from the integration which includes the diurnal cycle.

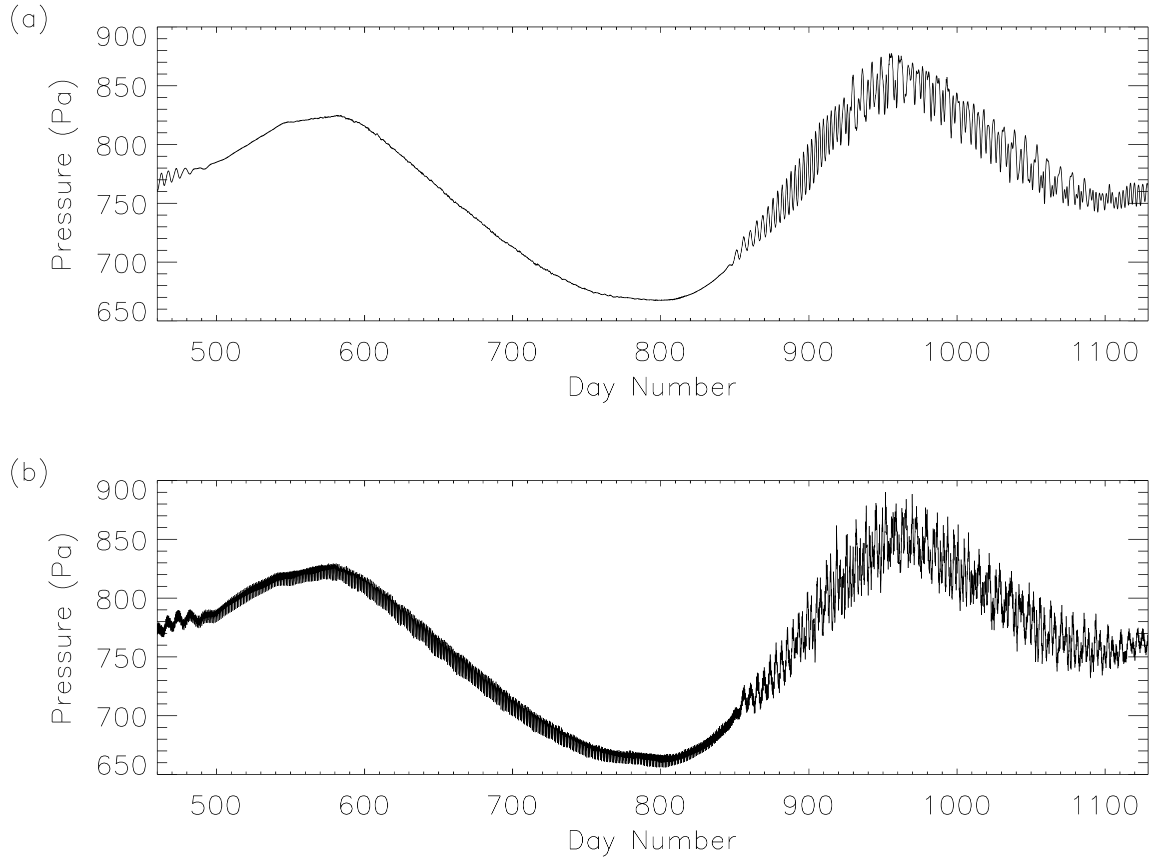

Figure 15: VL2 pressure from two years of simulation of the LMD Martian GCM. (a) A run with no diurnal cycle. (b) A run with the diurnal cycle included.

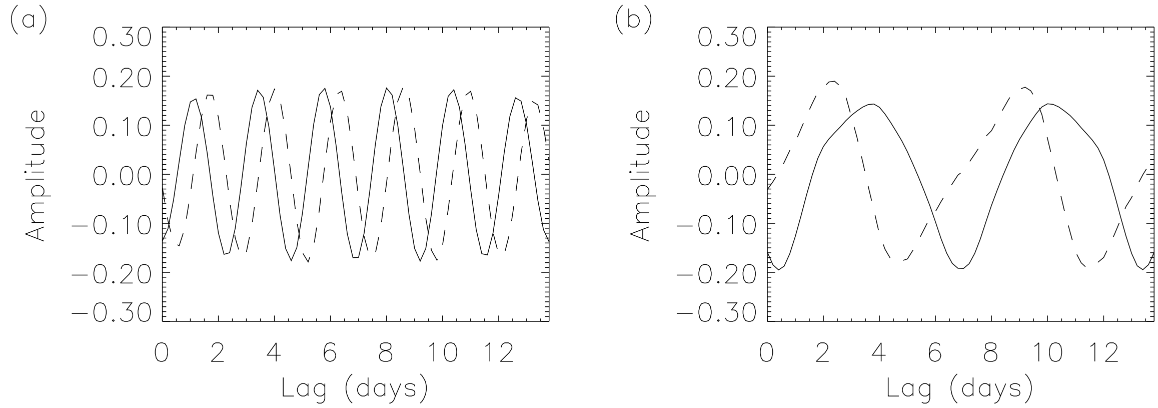

Figure 16: The top 4 eigenvectors computed from the detrended version of the data taken from 5 years of simulation of the LMD model with the diurnal cycle. (a) Eigenvector 1 (solid line), Eigenvector 2 (dashed line). (b) Eigenvector 3 (solid line), Eigenvector 4 (dashed line). A window length of 14 days was used.

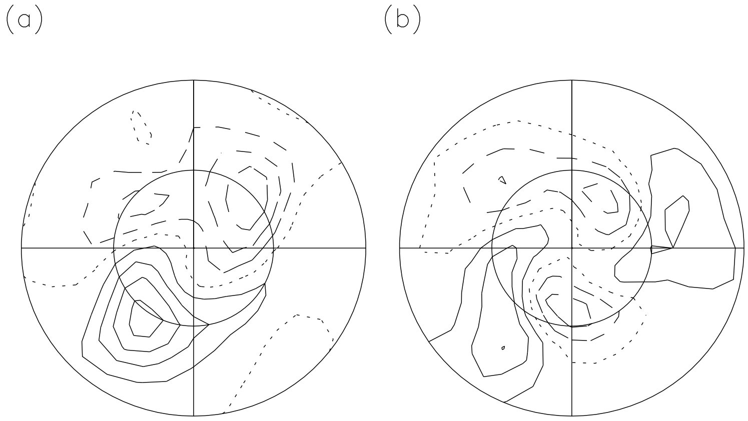

Figure 17: Snapshots of transient surface pressure anomaly from the LMD model corresponding to (a) the low frequency 6.7 day period wave and (b) the high frequency 2.4 day period wave. The projection and contour interval are the same as that shown in figures 11-14.

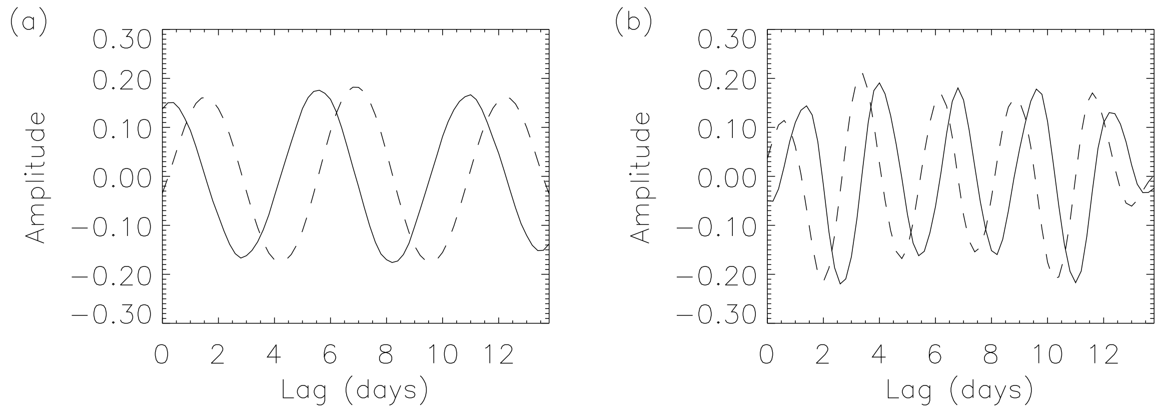

Figure 18: Eigenvectors computed from the detrended version of the data taken from 1 year of simulation of the $T21$, 20 level model.(a) Eigenvector 1 (solid line), Eigenvector 2 (dashed line). (b) Eigenvector 5 (solid line), Eigenvector 6 (dashed line). A window length of 14 days was used.